Int. J. Nanosci. Nanotechnol., Vol. 14, No. 3, Sept. 2018, pp. 207-227

Small Scale Effects on the Large Amplitude Nonlinear Vibrations of Multilayer Functionally Graded Composite Nanobeams Reinforced with Graphene-Nanoplatelets

Saeid Sahmani* **and Mohammad Mohammadi Aghdam**

Department of Mechanical Engineering, Amirkabir University of Technology, P.O. Box 15875-4413, Tehran, Iran.

(*) Corresponding author: sahmani@aut.ac.ir
(Received: 10 October 2017 and Accepted: 06 February 2018)

Abstract

The main purpose of the present investigation is to analyze more comprehensively the size-dependent nonlinear free vibration response of multilayer functionally graded graphene platelet-reinforced composite (GPLRC) nanobeams. As a consequence, both of the hardening stiffness and softening stiffness of size effect are taken into consideration by implementation of the nonlocal strain gradient elasticity theory within the framework of the third-order shear deformation beam theory. The graphene platelet (GPL) nanofillers are dispersed uniformly or in accordance with three different functionally graded patterns based on a layerwise change of their weight fraction through the individual layers. Halpin-Tsai micromechanical scheme is utilized to estimate the effective material properties of multilayer functionally graded GPLRC nanobeams. With the aid of the Hamilton's principle, the non-classical governing differential equations of motion are derived. After that, an improved perturbation technique in conjunction with the Galerkin method is employed to achieve an explicit analytical solution for nonlocal strain gradient nonlinear frequency of multilayer functionally graded GPLRC nanobeams. It is indicated that at zero vibration amplitude, the pattern of GPL dispersion has no influence on the significance of the size dependencies. However, by taking the large vibration amplitude into account, both of the nonlocality and strain gradient size effects on the nonlinear frequency of O-GPLRC and X-GPLRC nanobeams are minimum and maximum, respectively.

Keywords: *Nanostructures, Nanocomposites, Nonlinear dynamics, Graphene nanoplatelet, Nonlocal strain gradient elasticity.*

1. INRODUCTION

Similar to carbon nanotubes, graphene platelets (GPLs) have excellent performance characteristics in several applications [1, 2]. In opposite to graphene nanosheets, GPLs are available in a broad range of thickness from $0.34\ angstrom$ to $100\ nm$. Additionally, their high stiffness which is about 50 times stronger than steel in addition to having remarkable specific surface area that is twice that of carbon nanotube makes GPLs as one of the most efficient candidate to reinforce nanocomposite materials using in different technologies. For example, Ahmadi-Moghadam and Taheri [3] enhanced the interlaminar fracture toughness of fiber-reinforced polymer composites by including GPL nanofillers. Tang et al. [4] modified the form-phase change materials of plastic acid/high density polyethylene using GPLs as nanofillers. Scaffaro et al. [5] incorporated GPL as nanofiller in conjunction with ciprofloxacin as biocide into ploy lactic acid to create a biopolymer-based nanoomposites having antimicrobial properties. Yang et al. [6] achieved a great improvement in thermal conductivity as well as photoabsorption capability of poly ethylene glycol/ boron nitride composite by adding a very low content of GPL. Feng et al. [7] anticipated the nonlinear free vibration behavior of a

multilayer functionally graded composite beam reinforced with GPLs. Zhao et al. [8] explored the bending and vibration responses of FG trapezoidal plates reinforced with GPLs by employing the finite element method. Wang et al. [9] predicted the buckling behavior of cylindrical shells with cutouts reinforced with GPLs using finite element method. Feng et al. [10] investigated the effects of bi-axial stretching induced reorientation of GPLs on the Young's modulus of GPL/polymer composites using Mori-Tanaka micromechanics model. Sun et al. [11] studied the tensile behavior of polymer nanocomposites reinforced with GPLs in both zigzag and armchair directions via molecular dynamics simulations.

Recently, the mechanical characteristics of multilayer functional graded graphene platelet-reinforced composite (GPLRC) structures have been studied. Song et al. [12] reported the free and forced vibrational responses of multilayer functionally graded GPLRC plates on the basis of the first-order shear deformation plate theory. Feng et al. [13] investigated the nonlinear bending behavior of multilayer functionally graded GPLRC beams modeled by Timoshenko beam theory and van Karman nonlinear strain-displacement relationship. Yang et al. [14] analyzed the buckling and postbuckling characteristics of multilayer functionally graded GPLRC Timoshenko beams resting on an elastic medium.

Due to rapid advancement in materials science and technology, the miniaturized functionally graded composite materials can provide new opportunity for design of efficient micro- and nano-electromechanical systems and devices [15, 16]. As a result, size dependency in mechanical behaviors of these nanosized structures is worthy studying. In the last decade, various unconventional continuum elasticity theories have been put to use to capture different small scale effects on the mechanical characteristics of functionally graded nanostructures. Zhang et al. [17] presented a novel Mindlin plate element on the basis of the modified couple stress elasticity theory for size-dependent bending, vibration and buckling analysis of microplates. Akgoz and Civalek [18] analyzed free vibrations of axially functionally graded tapered Euler-Bernoulli microbeams using modified couple stress elasticity theory. Ramezani [19] used strain gradient elasticity theory to explore size effect on the nonlinear free vibration of microplates. Reddy et al. [20] developed the nonlinear finite element models of beam theories for bending of FG nanobeams based on nonlocal elasticity theory. Sahmani et al. [21] studied the postbuckling behavior of geometrically imperfect cylindrical nanoshells based on the surface elasticity theory. Shojaeian and Tadi Beni [22] explored the electromechanical buckling response of electrostatic nano-bridges. Li and Pan [23] constructed a size-dependent functionally graded piezoelectric plate model via couple stress theory of elasticity and sinusoidal plate theory. Jung et al. [24] solved static and eigenvalue problems for Sigmoid FG microplates using the modified couple stress elasticity theory. Sahmani et al. [25] employed Gurtin-Murdoch surface elasticity theory within the framework of third-order shear deformation beam theory to analyze free vibrations of postbuckled FG nanobeams. Kiani [26] established a nonlocal integro-differential model including surface free energy effects for free longitudinal vibration of FG nanorods. Sahmani et al. [27] anticipated the influence of the surface free energy on the axial postbuckling response of piezoelectric nanoshells. Mashrouteh et al. [28] investigated the higher modes of nonlinear free vibration of a fluid-conveying microtubes based on the modified couple stress theory. Sahmani and Aghdam [29] predicted the size-dependent nonlinear vibrations of pre- and post-buckled of FG composite nanobeams. Nguyen [30] used

the modified couple stress theory of elasticity to perform isogeometric analysis based on a novel quasi-3D shear deformation theory for size-dependent behaviors of FG microplates. Sahmani and Aghdam [31-33] employed the nonlocal strain gradient theory of elasticity to analyze the nonlinear instability of multilayer FG composite nanoplates and nanoshells under compressive mechanical load. Simsek and Aydin [34] predicted the size-dependent static bending and forced vibration of an imperfect functionally graded microplate via couple stress elasticity theory. Sahmani et al. [35] developed a size-dependent shell model based on the Gurtin-Murdoch elasticity theory to capture the surface free energy effect on the buckling behavior of silicon nanoshells. Sahmani and Fattahi [36] used molecular dynamics simulation to calibrate the constructed nonlocal plate for biaxial instability analysis of 3D metallic carbon nanosheets. They also employed the nonlocal theory of elasticity and surface elasticity to examine the mechanical characteristics of various nanostructures under different loading conditions [37-42].

Generally, in the previous investigations, it has been observed that the size effect in type of stress nonlocality has a softening-stiffness influence, while the strain gradient size dependency leads to a hardening-stiffness effect. Accordingly, Lim et al. [43] proposed a new size-dependent elasticity theory namely as nonlocal strain gradient theory which includes the both softening and stiffening influences to describe the size dependency in a more accurate way. Subsequently, a few studies have been performed on the basis of nonlocal strain gradient elasticity theory. Li and Hu [44] reported the size-dependent critical buckling loads of nonlinear Euler-Bernoulli nanobeams based upon nonlocal strain gradient theory of elasticity. They also presented the size-dependent frequency of wave motion on fluid-conveying carbon nanotubes via nonlocal strain gradient theory [45]. Yang et al. [46] established a nonlocal strain gradient beam model to evaluate the critical voltages corresponding to pull-in instability FG carbon nanotube reinforced actuators at nanoscale. Li et al. [47] developed a nonlocal strain gradient Timoshenko beam model for free vibration analysis of a nanobeam made of two-constituent FG material. Simsek [48] used nonlocal strain gradient theory to capture the size effects on the nonlinear natural frequencies of FGM Euler-Bernoulli nanobeams. Farajpour et al. [49] proposed a new size-dependent plate model for buckling of orthotropic nanoplates based on nonlocal strain gradient elasticity theory. Sahmani and Aghdam [50-52] utilized the nonlocal strain gradient theory of elasticity to analyze the size dependency in mechanical characteristics of the microtubule in a living ell. Lu et al. [53] implemented the nonlocal strain gradient theory of elasticity in the both Euler-Bernoulli and Timoshenko beam theories to analyze the bending and buckling behaviors of nanobeams. Sahmani and Aghdam [54] developed a nonlocal strain gradient shell model for size-dependent postbuckling analysis of magneto-electro-elastic composite nanoshells. Sahmani et al. [55,56] developed a nonlocal strain gradient plate model for the nonlinear instability and vibration responses of functionally graded porous micro/nano-plates reinforced with GPLs. Sahmani and Fattahi [57] employed the nonlocal strain gradient elasticity theory for buckling and postbuckling analysis of axially loaded functionally graded nanoshells. Moreover, the integral based nonlocal model has been also utilized in the nonlocal strain gradient elasticity. For instance, Zhu and Li [58,59] employed the integral based type of the nonlocal elasticity theory to analyze the mechanical characteristics as well as dynamics of rods at nanoscale.

In the current paper, size dependency in nonlinear vibrational response of multilayer functionally graded GPLRC nanobeams is studied. To this end, the

nonlocal strain gradient theory of elasticity is utilized within the third-order shear deformation beam theory. On the basis of the variational approach, the size-dependent governing differential equations of motion are constructed. Subsequently, a two-stepped perturbation technique in conjunction with the Galerkin method is employed to propose explicit analytical expressions for nonlocal strain gradient nonlinear frequency of multilayer functionally graded GPLRC nanobeams.

2. SIZE-DEPENDENT THIRD-ORDER SHEAR DEFORMABLE BEAM MODEL

In Figure 1, a six-layer functionally graded GPLRC nanobeam with length L, width b, thickness h and the attached coordinate system is illustrated schematically. The thicknesses of all six layers are assumed to be the same equal to $h_l = h/6$. For the multilayer functionally graded GPLRC nanobeam, the weight fraction of GPLs changes layerwise in accordance with a specific dispersion pattern. As it is shown in Figure 1, three different GPL dispersion patterns namely as X-GPLRC, O-GPLRC and A-GPLRC in addition to the uniform one (U-GPLRC) are taken into consideration. As a result, the GPL volume fraction of k-th layer corresponding to each type of the GPL dispersion pattern can be expressed as [7]

$$U-GPLRC: \quad V_{GPL}^{(k)} = V_{GPL}^{*}$$

$$X-GPLRC: \quad V_{GPL}^{(k)} = 2V_{GPL}^{*}\left(\frac{|2k-n_L-1|}{n_L}\right)$$

$$O-GPLRC: \quad V_{GPL}^{(k)} = 2V_{GPL}^{*}\left(1-\frac{|2k-n_L-1|}{n_L}\right)$$

$$A-GPLRC: \quad V_{GPL}^{(k)} = V_{GPL}^{*}\left(\frac{2k-1}{n_L}\right) \qquad (1)$$

where n_L denotes the total number of layers and V_{GPL}^{*} represents the total GPL volume fraction of nanobeam which can be evaluated as

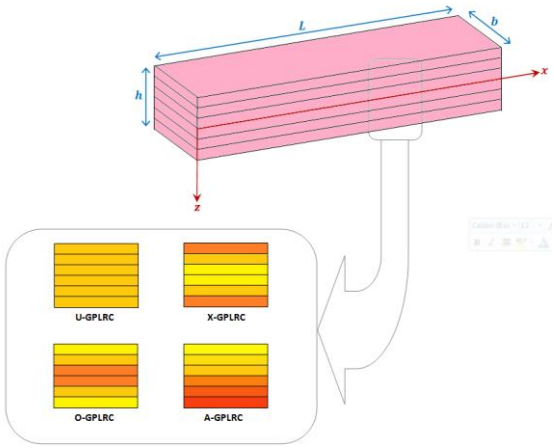

Figure 1. *Schematic representation of a multilayer GPLRC nanobeam with different patterns of GPL dispersion*

$$V_{GPL}^{*} = \frac{W_{GPL}}{W_{GPL} + \left(\frac{\rho_{GPL}}{\rho_m}\right)(1-W_{GPL})} \qquad (2)$$

in which ρ_{GPL} and ρ_m denote, respectively, the mass densities of GPLs and the polymer matrix of the nanobeam made from nanocomposite, and W_{GPL} is the GPL weight fraction.

In accordance with the Halpin-Tsai scheme [60], the Young's modulus relevant to k-th layer of the nanocomposite material with randomly oriented nanofillers can be extracted as

$$E^{(k)} = \left(\frac{3}{8}\frac{1+\lambda_L\eta_L V_{GPL}^{(k)}}{1-\eta_L V_{GPL}^{(k)}} + \frac{5}{8}\frac{1+\lambda_T\eta_T V_{GPL}^{(k)}}{1-\eta_T V_{GPL}^{(k)}}\right)E_m \qquad (3)$$

where E_m denotes the Young's modulus of the polymer matrix, and

$$\eta_L = \frac{\frac{E_{GPL}}{E_m}-1}{\frac{E_{GPL}}{E_m}+\lambda_L} \quad , \quad \eta_T = \frac{\frac{E_{GPL}}{E_m}-1}{\frac{E_{GPL}}{E_m}+\lambda_T}$$

$$\lambda_L = \frac{2L_{GPL}}{h_{GPL}} \quad , \quad \lambda_T = \frac{2b_{GPL}}{h_{GPL}} \qquad (4)$$

in which $E_{GPL}, L_{GPL}, b_{GPL}, h_{GPL}$ in order are the Young's modulus, length, width and thickness of GPL nanofiller.

On the other hand, based on the rule of mixture [61], the Poisson's ratio and mass density of the *k*-th layer of the multilayer functionally graded GPLRC nanobeam can be obtained as

$$\nu^{(k)} = \nu_m\left(1 - V_{GPL}^{(k)}\right) + \nu_{GPL}V_{GPL}^{(k)}$$

$$\rho^{(k)} = \rho_m\left(1 - V_{GPL}^{(k)}\right) + \rho_{GPL}V_{GPL}^{(k)} \quad (5)$$

in which ν_m and ν_{GPL} stand for the Poisson's ratios of the polymer matrix and GPL nanofiller, respectively.

Based upon the third-order shear deformation beam theory, the displacement components along different coordinate directions take the following forms

$$\begin{aligned} u_x(x,z,t) &= u(x,t) + z\psi(x,t) \\ &\quad - \frac{4z^3}{3h^2}\left(\psi(x,t) + \frac{\partial w(x,t)}{\partial x}\right) \\ u_y(x,z,t) &= 0 \\ u_z(x,z,t) &= w(x,t) \end{aligned} \quad (6)$$

where u, v and w are the displacement components of the multilayer functionally graded GPLRC nanobeam along *x*-, *y*- and *z*-axis, respectively. Additionally, ψ is the rotation relevant to the cross section of nanobeam at neutral plane normal about *y*-axis.

Subsequently, the non-zero strain components can be given as

$$\begin{aligned} \varepsilon_{xx} &= \varepsilon_{xx}^0 + z\left(\kappa_{xx}^{(0)} + z^2\kappa_{xx}^{(2)}\right) \\ &= \frac{\partial u}{\partial x} + \frac{1}{2}\left(\frac{\partial w}{\partial x}\right)^2 + z\frac{\partial \psi}{\partial x} \\ &\quad - \frac{4z^3}{3h^2}\left(\frac{\partial \psi}{\partial x} + \frac{\partial^2 w}{\partial x^2}\right) \\ \gamma_{xz} &= \gamma_{xz}^0 + z^2\kappa_{xz}^{(2)} \\ &= \psi + \frac{\partial w}{\partial x} - \frac{4z^2}{h^2}\left(\psi + \frac{\partial w}{\partial x}\right) \end{aligned} \quad (7)$$

in which $\varepsilon_{xx}^0, \gamma_{xz}^0$ represent the mid-plane strain components, $\kappa_{xx}^{(0)}$ is the first-order curvature component, and $\kappa_{xx}^{(2)}, \kappa_{xz}^{(2)}$ are the higher-order curvature components.

As it was mentioned before, both of the hardening-stiffness and stiffening-stiffness influences have been observed in the previous size-dependent analyses of nanostructures. Motivated by this fact, Lim et al. [43] proposed a new unconventional continuum theory namely as nonlocal strain gradient elasticity theory which takes simultaneously the nonlocal and strain gradient size effects into account. Therefore, the total nonlocal strain gradient stress tensor Λ for a beam-type structure can be expressed as below [43]

$$\Lambda_{xx} = \sigma_{xx} - \frac{\partial \sigma_{xx}^*}{\partial x} \quad (8a)$$

$$\Lambda_{xz} = \sigma_{xz} - \frac{\partial \sigma_{xz}^*}{\partial x} \quad (8b)$$

where σ and σ^* in order denote the stress and higher-order stress tensors which can be defined as

$$\begin{aligned} \sigma_{ij} &= \int_\Omega \left\{\varrho_1(|\mathcal{X}' - \mathcal{X}|)C_{ijkl}\varepsilon_{kl}(\mathcal{X}')\right\}d\Omega \\ \sigma_{ij}^* &= l^2\int_\Omega \left\{\varrho_2(|\mathcal{X}' - \mathcal{X}|)C_{ijkl}\frac{\partial \varepsilon_{kl}(\mathcal{X}')}{\partial x}\right\}d\Omega \end{aligned} \quad (9)$$

in which C is the elastic matrix, $\varrho_1$and ϱ_2 in order are the principal attenuation kernel function including the nonlocality and the additional kernel function associated with the nonlocality effect of the first-order strain gradient field, $\mathcal{X}$ and $\mathcal{X}'$ represent, respectively, a point and any point else in the body, and l stands for the internal strain gradient length scale parameter. Following the method of Eringen, the constitutive relationship corresponding to the total nonlocal strain gradient stress tensor of a beam-type structure can be written as

$$\left(1 - \mu^2\frac{\partial^2}{\partial x^2}\right)\Lambda_{ij} = C_{ijkl}\varepsilon_{kl} - l^2C_{ijkl}\frac{\partial^2 \varepsilon_{kl}}{\partial x^2} \quad (10)$$

in which μ represents the nonlocal parameter. Therefore, the nonlocal strain gradient constitutive relations for each individual layer k of a multilayer functionally graded GPLRC nanobeam can be expressed as

$$\left(1-\mu^2\frac{\partial^2}{\partial x^2}\right)\begin{Bmatrix}\sigma_{xx}\\ \sigma_{xz}\end{Bmatrix}_{(k)}$$
$$=\left(1-l^2\frac{\partial^2}{\partial x^2}\right)\begin{bmatrix}Q_{11}^{(k)} & 0\\ 0 & Q_{44}^{(k)}\end{bmatrix}\begin{Bmatrix}\varepsilon_{xx}\\ \gamma_{xz}\end{Bmatrix}_{(k)} \quad (11)$$

where

$$Q_{11}^{(k)}=\frac{E^{(k)}}{1-(\nu^{(k)})^2}\,,Q_{44}^{(k)}=\frac{E^{(k)}}{2(1+\nu^{(k)})} \quad (12)$$

Thus, within the framework of the nonlocal strain gradient third-order shear deformable beam model, the total strain energy of a multilayer functionally graded GPLRC nanobeam is as below

$$\Pi_s=\frac{1}{2}\int_0^L\int_{-\frac{h}{2}}^{\frac{h}{2}}\{\sigma_{ij}\varepsilon_{ij}+\sigma_{ij}^*\nabla\varepsilon_{ij}\}dz\,dx$$
$$=\frac{1}{2}\int_0^L\Big\{N_{xx}\varepsilon_{xx}^0+M_{xx}\kappa_{xx}^{(0)}+R_{xx}\kappa_{xx}^{(2)}$$
$$+Q_x\gamma_{xz}^0+S_x\kappa_{xz}^{(2)}\Big\}dx \quad (13)$$

where the stress resultants are in the following forms

$$N_{xx}-\mu^2\frac{\partial^2 N_{xx}}{\partial x^2}=A_{11}^*\left(\varepsilon_{xx}^0-l^2\frac{\partial^2\varepsilon_{xx}^0}{\partial x^2}\right)+B_{11}^*\left(\kappa_{xx}^{(0)}-l^2\frac{\partial^2\kappa_{xx}^{(0)}}{\partial x^2}\right)+D_{11}^*\left(\kappa_{xx}^{(2)}-l^2\frac{\partial^2\kappa_{xx}^{(2)}}{\partial x^2}\right)$$

$$M_{xx}-\mu^2\frac{\partial^2 M_{xx}}{\partial x^2}=B_{11}^*\left(\varepsilon_{xx}^0-l^2\frac{\partial^2\varepsilon_{xx}^0}{\partial x^2}\right)+C_{11}^*\left(\kappa_{xx}^{(0)}-l^2\frac{\partial^2\kappa_{xx}^{(0)}}{\partial x^2}\right)+F_{11}^*\left(\kappa_{xx}^{(2)}-l^2\frac{\partial^2\kappa_{xx}^{(2)}}{\partial x^2}\right)$$

$$R_{xx}-\mu^2\frac{\partial^2 R_{xx}}{\partial x^2}=D_{11}^*\left(\varepsilon_{xx}^0-l^2\frac{\partial^2\varepsilon_{xx}^0}{\partial x^2}\right)+F_{11}^*\left(\kappa_{xx}^{(0)}-l^2\frac{\partial^2\kappa_{xx}^{(0)}}{\partial x^2}\right)+H_{11}^*\left(\kappa_{xx}^{(2)}-l^2\frac{\partial^2\kappa_{xx}^{(2)}}{\partial x^2}\right)$$

$$Q_x-\mu^2\frac{\partial^2 Q_x}{\partial x^2}=A_{44}^*\left(\gamma_{xz}^0-l^2\frac{\partial^2\gamma_{xz}^0}{\partial x^2}\right)+C_{44}^*\left(\kappa_{xz}^{(2)}-l^2\frac{\partial^2\kappa_{xz}^{(2)}}{\partial x^2}\right)$$

$$S_x-\mu^2\frac{\partial^2 S_x}{\partial x^2}=C_{44}^*\left(\gamma_{xz}^0-l^2\frac{\partial^2\gamma_{xz}^0}{\partial x^2}\right)+F_{44}^*\left(\kappa_{xz}^{(2)}-l^2\frac{\partial^2\kappa_{xz}^{(2)}}{\partial x^2}\right) \quad (14)$$

in which

$$\{N_{xx},M_{xx},R_{xx}\}=\sum_{k=1}^{n_L}\left(\int_{z_{k-1}}^{z_k}\Lambda_{xx}^{(k)}\{1,z,z^3\}dz\right)$$
$$\{Q_x,S_x\}=\sum_{k=1}^{n_L}\left(\int_{z_{k-1}}^{z_k}\Lambda_{xz}^{(k)}\{1,z^2\}dz\right) \quad (15)$$

and

$$\{A_{11}^*,B_{11}^*,C_{11}^*,D_{11}^*,F_{11}^*,H_{11}^*\}=b\sum_{k=1}^{n_L}\left(Q_{11}^{(k)}\int_{z_{k-1}}^{z_k}\{1,z,z^2,z^3,z^4,z^6\}dz\right)$$

$$\{A_{44}^*,C_{44}^*,F_{44}^*\}=b\sum_{k=1}^{n_L}\left(Q_{44}^{(k)}\int_{z_{k-1}}^{z_k}\{1,z^2,z^4\}dz\right) \quad (16)$$

Also, the kinetic energy of a multilayer functionally graded GPLRC nanobeam modeled via the nonlocal strain gradient third-order shear deformable beam model can be expressed as

$$\Pi_T=\frac{1}{2}\int_0^L\int_{-\frac{h}{2}}^{\frac{h}{2}}\rho\left\{\left(\frac{\partial u_x}{\partial t}\right)^2+\left(\frac{\partial u_z}{\partial t}\right)^2\right\}dz\,dx$$
$$=\frac{1}{2}\int_0^L\Bigg\{I_0\left(\frac{\partial u}{\partial t}\right)^2-\frac{8}{3h^2}I_3\frac{\partial u}{\partial t}\frac{\partial^2 w}{\partial x\partial t}$$
$$+\left(2I_1-\frac{8}{3h^2}I_3\right)\frac{\partial u}{\partial t}\frac{\partial\psi}{\partial t}+\frac{16}{9h^4}I_6\left(\frac{\partial^2 w}{\partial x\partial t}\right)^2$$
$$+\left(\frac{16}{9h^4}I_6-\frac{4}{3h^2}I_4\right)\frac{\partial^2 w}{\partial x\partial t}\frac{\partial\psi}{\partial t}$$
$$+\left(I_2-\frac{8}{3h^2}I_4+\frac{16}{9h^4}I_6\right)\left(\frac{\partial\psi}{\partial t}\right)^2$$
$$+I_0\left(\frac{\partial w}{\partial x}\right)^2\Bigg\}dx \quad (17)$$

where

$$\{I_0, I_1, I_2, I_3, I_4, I_6\} = b\sum_{k=1}^{n_L}\left(\rho^{(k)}\int_{z_{k-1}}^{z_k}\{1, z, z^2, z^3, z^4, z^6\}dz\right) \quad (18)$$

In addition, the work done by the transverse force q can be introduced as follows

$$\Pi_w = \int_0^L q(x,t)w dx \quad (19)$$

Now, with the aid of the Hamilton's principle, the governing differential equations in terms of stress resultants can be derived as

$$\frac{\partial N_{xx}}{\partial x} = I_0\frac{\partial^2 u}{\partial t^2} - \frac{4}{3h^2}I_3\frac{\partial^3 w}{\partial x \partial t^2} + \left(I_1 - \frac{4}{3h^2}I_3\right)\frac{\partial^2 \psi}{\partial t^2} \quad (20a)$$

$$\frac{4}{3h^2}\frac{\partial^2 R_{xx}}{\partial x^2} + \frac{4}{h^2}\frac{\partial Q_x}{\partial x} - \frac{4}{h^2}\frac{\partial S_x}{\partial x} + \frac{\partial N_{xx}}{\partial x}\frac{\partial w}{\partial x} + \frac{\partial}{\partial x}\left(N_{xx}\frac{\partial w}{\partial x}\right) + q = \frac{4}{3h^2}I_3\frac{\partial^2 u}{\partial t^2} + I_0\frac{\partial^2 w}{\partial t^2} - \frac{16}{9h^4}I_6\frac{\partial^4 w}{\partial x^2 \partial t^2} + \left(\frac{4}{3h^2}I_4 - \frac{16}{9h^4}I_6\right)\frac{\partial^3 \psi}{\partial x \partial t^2} \quad (20b)$$

$$\frac{\partial M_{xx}}{\partial x} - \frac{4}{3h^2}\frac{\partial R_{xx}}{\partial x} - \frac{4}{h^2}Q_x + \frac{4}{h^2}S_x = \left(I_1 - \frac{4}{3h^2}I_3\right)\frac{\partial^2 u}{\partial t^2} - \left(\frac{4}{3h^2}I_4 - \frac{16}{9h^4}I_6\right)\frac{\partial^3 w}{\partial x \partial t^2} + \left(I_2 - \frac{8}{3h^2}I_4 + \frac{16}{9h^4}I_6\right)\frac{\partial^2 \psi}{\partial t^2} \quad (20c)$$

After that, by substitution equation (20a) in equations (20b) and (20c), and using equation (14), the nonlocal strain gradient governing differential equations of motion for a multilayer functionally graded GPLRC third-order shear deformable nanobeam with immovable end conditions take the following form

$$\left(1 - l^2\frac{\partial^2}{\partial x^2}\right)\left(\varphi_1\frac{\partial^4 w}{\partial x^4} - \varphi_2\frac{\partial^3 \psi}{\partial x^3}\right) = \left(1 - \mu^2\frac{\partial^2}{\partial x^2}\right)\left(q + N_{xx}\frac{\partial^2 w}{\partial x^2} - I_0\frac{\partial^2 w}{\partial t^2} + I_1^*\frac{\partial^4 w}{\partial x^2 \partial t^2} - I_2^*\frac{\partial^3 \psi}{\partial x \partial t^2}\right) \quad (21a)$$

$$\varphi_3\frac{\partial^3 w}{\partial x^3} + \varphi_4\frac{\partial^2 \psi}{\partial x^2} - \varphi_5\left(\psi + \frac{\partial w}{\partial x}\right) = I_3^*\frac{\partial^3 w}{\partial x \partial t^2} + I_4^*\frac{\partial^2 \psi}{\partial t^2} \quad (21b)$$

$$N_{xx} = \frac{1}{L}\int_0^L\left\{\frac{A_{11}^*}{2}\left(\frac{\partial w}{\partial x}\right)^2 + B_{11}^*\frac{\partial \psi}{\partial x} - \frac{4D_{11}^*}{3h^2}\left(\frac{\partial \psi}{\partial x} + \frac{\partial^2 w}{\partial x^2}\right)\right\}dx \quad (21c)$$

in which

$$\varphi_1 = \frac{4}{3h^2}\left(F_{11}^* - \frac{B_{11}^* D_{11}^*}{A_{11}^*}\right)$$

$$\varphi_2 = C_{11}^* - \frac{(B_{11}^*)^2}{A_{11}^*} - \frac{4}{3h^2}\left(F_{11}^* - \frac{B_{11}^* D_{11}^*}{A_{11}^*}\right)$$

$$\varphi_3 = -\frac{4}{3h^2}\left(F_{11}^* - \frac{B_{11}^* D_{11}^*}{A_{11}^*} - \frac{4}{3h^2}\left(H_{11}^* - \frac{(D_{11}^*)^2}{A_{11}^*}\right)\right)$$

$$\varphi_4 = C_{11}^* - \frac{(B_{11}^*)^2}{A_{11}^*} - \frac{8}{3h^2}\left(F_{11}^* - \frac{B_{11}^* D_{11}^*}{A_{11}^*}\right) - \frac{16}{9h^4}\left(H_{11}^* - \frac{(D_{11}^*)^2}{A_{11}^*}\right)$$

$$\varphi_5 = A_{44}^* - \frac{8}{h^2}C_{44}^* + \frac{16}{h^4}F_{44}^*$$

$$I_1^* = \frac{4}{3h^2}\left(I_4 - \frac{I_1 I_3}{I_0}\right) \quad (22)$$

$$I_2^* = I_2 - \frac{I_1^2}{I_0} - \frac{4}{3h^2}\left(I_4 - \frac{4}{3h^2}\frac{I_1 I_3}{I_0}\right)$$

$$I_3^* = I_2 - \frac{I_1^2}{I_0} - \frac{8}{3h^2}\left(I_4 - \frac{I_1 I_3}{I_0}\right) + \frac{16}{9h^4}\left(I_6 - \frac{I_3^2}{I_0}\right)$$

$$I_4^* = -\frac{4}{3h^2}\left(I_4 - \frac{I_1 I_3}{I_0}\right) + \frac{16}{9h^4}\left(I_6 - \frac{I_3^2}{I_0}\right)$$

3. ANALYTICAL SOLVING PROCESS FOR ASYMPTATIC SOLUTIONS

Before starting the solving process, in order to achieve the asymptotic solutions for the size-dependent problem, the following dimensionless parameters are taken into account

$$X=\frac{\pi x}{L}\quad,\quad W=\frac{w}{L}\quad,\quad \Psi=\frac{\psi}{\pi}$$

$$\tau=\frac{\pi t}{L}\sqrt{\frac{A_{00}}{I_{00}}}\quad,\quad \mathcal{P}_q=\frac{q_0L^3}{\pi^4A_{00}h^2}$$

$$\{a_{11}^*,b_{11}^*,c_{11}^*,d_{11}^*,f_{11}^*,h_{11}^*\}=\left\{\frac{L^2A_{11}^*}{\pi^2A_{00}h^2},\frac{LB_{11}^*}{\pi A_{00}h^2},\frac{C_{11}^*}{A_{00}h^2},\frac{LD_{11}^*}{\pi A_{00}h^4},\frac{F_{11}^*}{A_{00}h^4},\frac{H_{11}^*}{A_{00}h^6}\right\}$$

$$\{a_{44}^*,c_{44}^*,f_{44}^*\}=\left\{\frac{A_{44}^*}{A_{00}},\frac{C_{44}^*}{A_{00}h^2},\frac{F_{44}^*}{A_{00}h^4}\right\}$$

$$\mathcal{G}_1=\frac{\mu}{L}\quad,\quad \mathcal{G}_2=\frac{l}{L} \tag{23}$$

$$\{\vartheta_1,\vartheta_2,\vartheta_3,\vartheta_4,\vartheta_5\}=\left\{\frac{\varphi_1}{A_{00}h^2},\frac{\varphi_2}{A_{00}h^2},\frac{\varphi_3}{A_{00}h^2},\frac{\varphi_4}{A_{00}h^2},\frac{L^2\varphi_5}{\pi^2A_{00}h^2}\right\}$$

$$\{\bar{I}_0,\bar{I}_1,\bar{I}_2,\bar{I}_3,\bar{I}_4,\bar{I}_6\}=\left\{\frac{L^2I_0}{\pi^2I_{00}h^2},\frac{LI_1}{\pi I_{00}h^2},\frac{I_2}{I_{00}h^2},\frac{LI_3}{\pi I_{00}h^4},\frac{I_4}{I_{00}h^4},\frac{I_6}{I_{00}h^6}\right\}$$

where $A_{00}=E_mbh$ and $I_{00}=\rho_mbh$. Consequently, the nonlocal strain gradient governing differential equations of motion for third-order shear deformable multilayer functionally graded GPLRC nanobeam can be rewritten in dimensionless form as below

$$\left(1-\pi^2\mathcal{G}_2^2\frac{\partial^2}{\partial X^2}\right)\left(\vartheta_1\frac{\partial^4W}{\partial X^4}-\vartheta_2\frac{\partial^3\Psi}{\partial X^3}\right)=\left(1-\pi^2\mathcal{G}_1^2\frac{\partial^2}{\partial X^2}\right)\left[\mathcal{P}_q-\bar{I}_0\frac{\partial^2W}{\partial\tau^2}+\bar{I}_1^*\frac{\partial^4W}{\partial X^2\partial\tau^2}-\bar{I}_2^*\frac{\partial^3\Psi}{\partial X\partial\tau^2}+\pi\left(\int_0^\pi\left\{\frac{a_{11}^*}{2}\left(\frac{\partial W}{\partial X}\right)^2+b_{11}^*\frac{\partial\Psi}{\partial X}-\frac{4d_{11}^*}{3}\left(\frac{\partial\Psi}{\partial X}+\frac{\partial^2W}{\partial X^2}\right)\right\}dX\right)\frac{\partial^2W}{\partial X^2}\right] \tag{24a}$$

$$\vartheta_3\frac{\partial^3W}{\partial X^3}+\vartheta_4\frac{\partial^2\Psi}{\partial X^2}-\vartheta_5\left(\Psi+\frac{\partial W}{\partial X}\right)=\bar{I}_3^*\frac{\partial^3W}{\partial X\partial\tau^2}+\bar{I}_4^*\frac{\partial^2\Psi}{\partial\tau^2} \tag{24b}$$

To continue the solution methodology, an improved perturbation method namely as two-stepped perturbation technique [62-72] is employed. To accomplish this purpose, the independent variables are considered as the summations of the solutions corresponding to different orders of the first perturbation parameter, ϵ, as below

$$\bar{W}(X,\hat{\tau},\epsilon)=\sum_{i=1}\epsilon^i\bar{W}_i(X,\hat{\tau})$$

$$\bar{\Psi}(X,\hat{\tau},\epsilon)=\sum_{i=1}\epsilon^i\bar{\Psi}_i(X,\hat{\tau}) \tag{25}$$

where $\hat{\tau}=\epsilon\tau$ is taken into account to improve the efficiency of the perturbation approach for capturing the solution of vibration problem. In such a case, the nonlocal strain gradient governing differential equations of motion become

$$\left(1-\pi^2\mathcal{G}_2^2\frac{\partial^2}{\partial X^2}\right)\left(\vartheta_1\frac{\partial^4\bar{W}}{\partial X^4}-\vartheta_2\frac{\partial^3\bar{\Psi}}{\partial X^3}\right)=\left(1-\pi^2\mathcal{G}_1^2\frac{\partial^2}{\partial X^2}\right)\left[\mathcal{P}_q-\epsilon^2\left(\bar{I}_0\frac{\partial^2\bar{W}}{\partial\hat{\tau}^2}-\bar{I}_1^*\frac{\partial^4\bar{W}}{\partial X^2\partial\hat{\tau}^2}+\bar{I}_2^*\frac{\partial^3\bar{\Psi}}{\partial X\partial\hat{\tau}^2}\right)+\pi\left(\int_0^\pi\left\{\frac{a_{11}^*}{2}\left(\frac{\partial W}{\partial X}\right)^2+b_{11}^*\frac{\partial\Psi}{\partial X}-\frac{4d_{11}^*}{3}\left(\frac{\partial\Psi}{\partial X}+\frac{\partial^2W}{\partial X^2}\right)\right\}dX\right)\frac{\partial^2W}{\partial X^2}\right] \tag{26a}$$

$$\vartheta_3\frac{\partial^3\bar{W}}{\partial X^3}+\vartheta_4\frac{\partial^2\bar{\Psi}}{\partial X^2}-\vartheta_5\left(\bar{\Psi}+\frac{\partial\bar{W}}{\partial X}\right)=\epsilon^2\left(\bar{I}_3^*\frac{\partial^3\bar{W}}{\partial X\partial\hat{\tau}^2}+\bar{I}_4^*\frac{\partial^2\bar{\Psi}}{\partial\hat{\tau}^2}\right) \tag{26b}$$

It is assumed that the immovable ends of multilayer functionally graded GPLRC

nanobeams are simply supported and the initial conditions are as follow

$$\bar{W}|_{\hat{\tau}=0} = 0 \quad , \quad \left.\frac{\partial \bar{W}}{\partial \hat{\tau}}\right|_{\hat{\tau}=0} = 0$$

$$\bar{\Psi}|_{\hat{\tau}=0} = 0 \quad , \quad \left.\frac{\partial \bar{\Psi}}{\partial \hat{\tau}}\right|_{\hat{\tau}=0} = 0 \qquad (27)$$

By inserting equation (25) in equations (26a) and (26b) and then collecting the expressions with the same order of ϵ, a set of perturbation equations is extracted. Afterwards, the asymptotic solutions corresponding to each individual variable can be obtained as

$$\bar{W}(X,\tau,\epsilon) = \epsilon A_{10}^{(1)}(\tau)\sin(mX) + O(\epsilon^4)$$

$$\bar{\Psi}(X,\tau,\epsilon) = \epsilon B_{10}^{(1)}(\tau)\sin(mX) + \epsilon^3 B_{10}^{(3)}\cos(mX) + O(\epsilon^4) \qquad (28)$$

$$\mathcal{P}_q(X,\tau,\epsilon) = \left[\left(\frac{m^4\xi_2}{\xi_1}\left(\vartheta_1 + \vartheta_2\frac{\vartheta_3 m^2+\vartheta_5}{\vartheta_4 m^2+\vartheta_5}\right)\right)\left(\epsilon A_{10}^{(1)}(\tau)\right) + \left(\bar{I}_0 + m^2\left(\bar{I}_1^* + \frac{\bar{I}_2^*\xi_2}{\xi_1}\frac{\vartheta_3 m^2+\vartheta_5}{\vartheta_4 m^2+\vartheta_5}\right) - \frac{\vartheta_3 m^4\xi_2}{(\vartheta_4 m^2+\vartheta_5)\xi_1}\left(\bar{I}_3^* - \bar{I}_4^*\frac{\vartheta_3 m^2+\vartheta_5}{\vartheta_4 m^2+\vartheta_5}\right)\right)\frac{\partial^2\left(\epsilon A_{10}^{(1)}(\tau)\right)}{\partial\tau^2}\right]\sin(mX) + \left(\frac{\pi^2 m^4 a_{11}^*}{4}\right)\left(\epsilon A_{10}^{(1)}(\tau)\right)^3\sin(mX) + O(\epsilon^4)$$

where

$$\xi_1 = 1 + \pi^2 m^2 \mathcal{G}_1^2$$

$$\xi_2 = 1 + \pi^2 m^2 \mathcal{G}_2^2 \qquad (29)$$

Related to the free vibration analysis, one will have $\mathcal{P}_q = 0$. As a result, after applying the Galerkin method, it yields

$$\left[\frac{m^4\xi_2}{\xi_1}\left(\vartheta_1 + \vartheta_2\frac{\vartheta_3 m^2+\vartheta_5}{\vartheta_4 m^2+\vartheta_5}\right)\right]\left(\epsilon A_{10}^{(1)}(\tau)\right) + \left[\bar{I}_0 + m^2\left(\bar{I}_1^* + \frac{\bar{I}_2^*\xi_2}{\xi_1}\frac{\vartheta_3 m^2+\vartheta_5}{\vartheta_4 m^2+\vartheta_5}\right) - \frac{\vartheta_3 m^4\xi_2}{(\vartheta_4 m^2+\vartheta_5)\xi_1}\left(\bar{I}_3^* - \bar{I}_4^*\frac{\vartheta_3 m^2+\vartheta_5}{\vartheta_4 m^2+\vartheta_5}\right)\right]\frac{\partial^2\left(\epsilon A_{10}^{(1)}(\tau)\right)}{\partial\tau^2} + \left(\frac{\pi^2 m^4 a_{11}^*}{4}\right)\left(\epsilon A_{10}^{(1)}(\tau)\right)^3 = 0 \qquad (30)$$

As a consequence, the nonlinear nonlocal strain gradient frequency of the multilayer functionally graded GPLRC nanobeam can be calculated by an explicit analytical expression as follows

$$\omega_{NL} = \omega_L\sqrt{1 + \frac{3\left(\frac{\pi^2 m^4 a_{11}^*}{4}\right)}{4\left[\frac{m^4\xi_2}{\xi_1}\left(\vartheta_1 + \vartheta_2\frac{\vartheta_3 m^2+\vartheta_5}{\vartheta_4 m^2+\vartheta_5}\right)\right]}W_{max}^2} \qquad (31)$$

where the linear nonlocal strain gradient natural frequency can be defined as

$$\omega_L = \sqrt{\frac{\frac{m^4\xi_2}{\xi_1}\left(\vartheta_1 + \vartheta_2\frac{\vartheta_3 m^2+\vartheta_5}{\vartheta_4 m^2+\vartheta_5}\right)}{\bar{I}_0 + m^2\left(\bar{I}_1^* + \frac{\bar{I}_2^*\xi_2}{\xi_1}\frac{\vartheta_3 m^2+\vartheta_5}{\vartheta_4 m^2+\vartheta_5}\right) - \frac{\vartheta_3 m^4\xi_2}{(\vartheta_4 m^2+\vartheta_5)\xi_1}\left(\bar{I}_3^* - \bar{I}_4^*\frac{\vartheta_3 m^2+\vartheta_5}{\vartheta_4 m^2+\vartheta_5}\right)}} \qquad (32)$$

and W_{max} stands for the dimensionless maximum deflection of nanobeam.

4. NUMERICAL RESULTS AND DISCUSSION

The geometric parameters of the multilayer functionally graded GPLRC nanobeams are selected as $h = 3\,nm$ for $n_L =$, $b = h$, $L = 20h$, $h_{GPL} = 0.34\,nm$, $L_{GPL} = 5\,nm$, and $b_{GPL} = 2.5\,nm$. The material properties of the polymer matrix and GPL nanofillers are given in Table 1.

Firstly, the validity as well as the accuracy of the present solution methodology is checked.

Table 1. *Material properties of the polymer matrix and GPL nanofillers [73,74].*

$E_{GPL}\ (TPa)$	1.01
ν_{GPL}	0.186
$\rho_{GPL}\ (Kg/m^3)$	1062.5
$E_m\ (GPa)$	3
ν_m	0.34
$\rho_m\ (Kg/m^3)$	1200

Table 2. *Comparison of nonlocal nonlinear frequency ratios (ω_{NL}/ω_L) for an isotropic homogenous simply supported nanobeam corresponding to different maximum deflections ($\mathcal{G}_1 = 0.15$).*

$w_{max}/\sqrt{I/A}$	Present solution	Ref. [75]
1	1.10662	1.11920
2	1.40244	1.41801
3	1.78701	1.80919
4	2.22994	2.24511
5	2.69028	2.70429

In accordance with the best authors' knowledge, there is no investigation in which the nonlocal strain gradient nonlinear vibration of nanobeams is studied. Therefore, in Table 2, the nonlocal nonlinear frequency ratio (ω_{NL}/ω_L) for an isotropic homogeneous simply supported nanobeam is given and compared with those presented by Yang et al. [75] using differential quadrature method. A very good agreement is found which confirms the validity as well as accuracy of the present solution methodology.

Presented in Figure 2 is the dimensionless variation of nonlinear frequency to linear frequency ratio with maximum deflection (vibration amplitude) of multilayer functionally graded GPLRC nanobeam corresponding to different small scale parameters. It can be observed that the nonlocality causes to increase the slope of variation, while the strain gradient size dependency leads to reduce it. Furthermore, it is revealed that by moving to deeper nonlinear regime (increasing the vibration amplitude of nanobeam), both types of the small scale effect plays more important role in the value of nonlinear frequency to linear frequency ratio of multilayer functionally graded GPLRC nanobeams, so the gap between different curves increases.

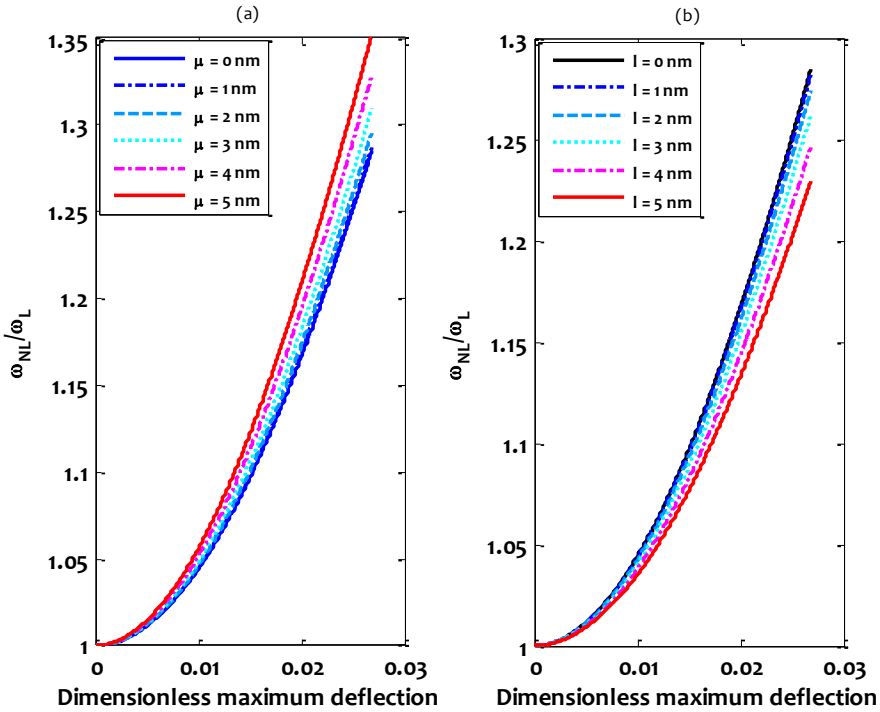

Figure 2. *Variation of nonlinear frequency to linear frequency ratio with vibration amplitude of multilayer U-GPLRC nanobeams corresponding to various small scale parameters ($V_{GPL}^{*} = 0.3$): (a) $l = 0\ nm$, (b) $\mu = 0\ nm$.*

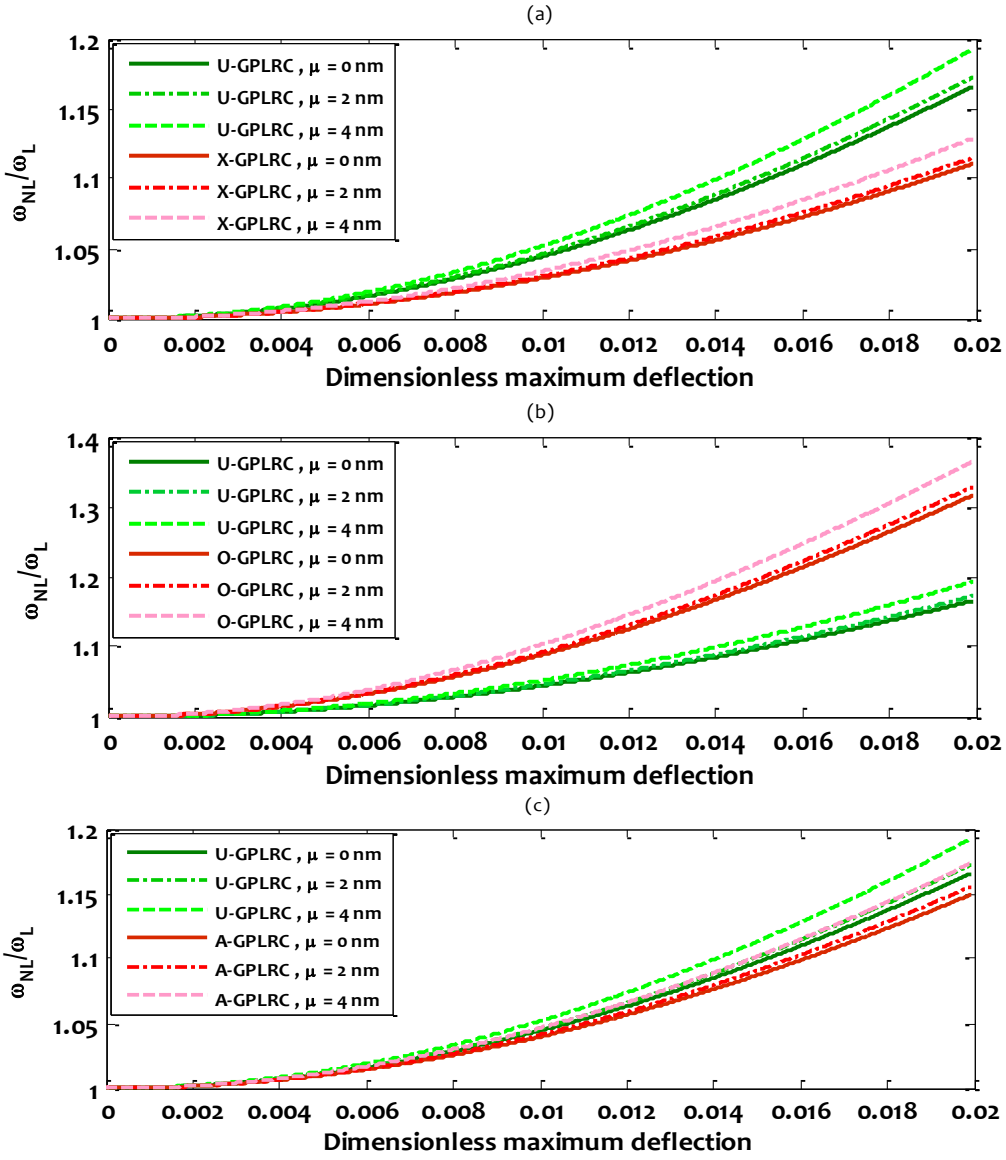

Figure 3. *Variation of nonlinear frequency to linear frequency ratio with vibration amplitude of multilayer functionally graded GPLRC nanobeams corresponding to various small scale parameters and GPL dispersion patterns ($V_{GPL}^{*} = 0.3, l = 0\ nm$).*

Figures 3 and 4 depict the dimensionless variation of nonlinear frequency to linear frequency ratio with the maximum deflection (vibration amplitude) of multilayer functionally graded GPLRC nanobeams with various GPL dispersion patterns including nonlocality size effect and strain gradient size dependency, respectively. It can be seen that among different patterns of GPL dispersion, for X-GPLRC and O-GPLRC nanobeams, the slope of variation of the frequency ratio with vibration amplitude of nanobeams becomes, respectively, minimum and maximum. In other words, by changing the dispersion pattern from uniform one to X-

GPLRC and O-GPLRC ones, the role of geometrical nonlinearity on the free vibration behavior of the multilayer functionally graded nanobeam decreases and increases, respectively. This anticipation is similar corresponding to both of the small scale effects with different values.

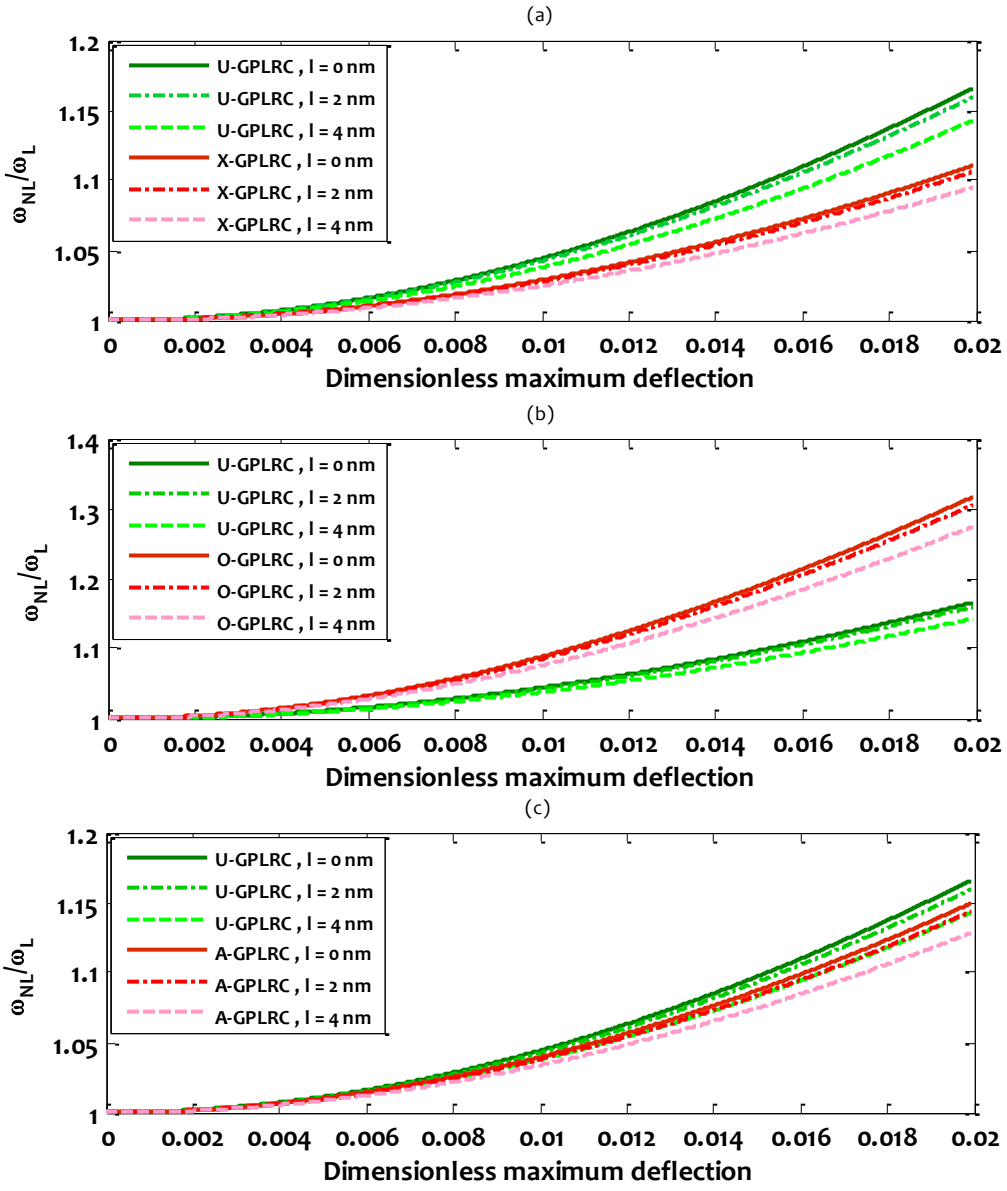

Figure 4. *Variation of nonlinear frequency to linear frequency ratio with vibration amplitude of multilayer functionally graded GPLRC nanobeams corresponding to various small scale parameters and GPL dispersion patterns* ($V^*_{GPL} = 0.3, \mu = 0\ nm$).

In Table 3, the dimensionless nonlinear frequency of multilayer functionally graded GPLRC nanobeams with different patterns of GPL dispersion and corresponding to various values of vibration amplitude and small scale parameters. The percentages given in parentheses represent the difference between the size-dependent and the classical ($\mu = l = 0\ nm$) nonlinear frequencies. It is revealed that for all GPL dispersion patterns and various vibration amplitudes, the strain gradient size effect on the nonlinear frequency of GPLRC nanobeams is a bit more than that of nonlocality with the same value of small

scale parameter. Furthermore, it is seen that at zero vibration amplitude, the pattern of GPL dispersion has no influence on the significance of the size dependencies, so the percentages are similar corresponding to each value of small scale parameter. However, by taking the large vibration amplitude into account, both of the nonlocality and strain gradient size effects on the nonlinear frequency of O-GPLRC and X-GPLRC nanobeams are minimum and maximum, respectively.

Table 3. *Size-dependent dimensionless nonlinear frequencies of multilayer GPLRC nanobeams with different patterns of GPL dispersion and corresponding to various small scale parameters and vibrations amplitudes ($V^*_{GPL} = 0.3$).*

Small scale parameters	U-GPLRC	X-GPLRC	O-GPLRC	A-GPLRC
$W_{max} = 0$, $l = 0\ nm$				
$\mu = 0\ nm$	0.1628	0.2190	0.1233	0.1882
$\mu = 1\ nm$	0.1619 (-0.544%)	0.2175 (-0.544%)	0.1226 (-0.544%)	0.1871 (-0.544%)
$\mu = 2\ nm$	0.1594 (-2.125%)	0.2143 (-2.125%)	0.1207 (-2.125%)	0.1842 (-2.125%)
$\mu = 3\ nm$	0.1553 (-4.597%)	0.2089 (-4.597%)	0.1176 (-4.597%)	0.1795 (-4.597%)
$\mu = 4\ nm$	0.1502 (-7.765%)	0.2020 (-7.765%)	0.1137 (-7.765%)	0.1735 (-7.765%)
$W_{max} = 0.01$, $l = 0\ nm$				
$\mu = 0\ nm$	0.1700	0.2253	0.1342	0.1956
$\mu = 1\ nm$	0.1692 (-0.499%)	0.2241 (-0.514%)	0.1335 (-0.459%)	0.1946 (-0.503%)
$\mu = 2\ nm$	0.1667 (-1.947%)	0.2208 (-2.006%)	0.1318 (-1.791%)	0.1918 (-1.964%)
$\mu = 3\ nm$	0.1629 (-4.209%)	0.2155 (-4.338%)	0.1290 (-3.869%)	0.1873 (-4.248%)
$\mu = 4\ nm$	0.1580 (-7.099%)	0.2088 (-7.320%)	0.1254 (-6.516%)	0.1816 (-7.165%)
$W_{max} = 0.02$, $l = 0\ nm$				
$\mu = 0\ nm$	0.1900	0.2433	0.1625	0.2164
$\mu = 1\ nm$	0.1892 (-0.399%)	0.2422 (-0.441%)	0.1620 (-0.313%)	0.2155 (-0.411%)
$\mu = 2\ nm$	0.1870 (-1.558%)	0.2391 (-1.720%)	0.1605 (-1.219%)	0.2130 (-1.603%)
$\mu = 3\ nm$	0.1836 (-3.360%)	0.2343 (-3.712%)	0.1582 (-2.624%)	0.2089 (-3.459%)
$\mu = 4\ nm$	0.1793 (-5.650%)	0.2281 (-6.249%)	0.1553 (-4.399%)	0.2038 (-5.819%)
$W_{max} = 0$, $\mu = 0\ nm$				
$l = 0\ nm$	0.1628	0.2190	0.1233	0.1882
$l = 1\ nm$	0.1637 (+0.547%)	0.2202 (+0.547%)	0.1239 (+0.547%)	0.1892 (+0.547%)
$l = 2\ nm$	0.1664 (+2.170%)	0.2237 (+2.170%)	0.1259(+2.170%)	0.1922 (+2.170%)
$l = 3\ nm$	0.1707 (+4.819%)	0.2295 (+4.819%)	0.1292 (+4.819%)	0.1972 (+4.819%)
$l = 4\ nm$	0.1765 (+8.419%)	0.2374 (+8.419%)	0.1337 (+8.419%)	0.2040 (+8.419%)
$W_{max} = 0.01$, $\mu = 0\ nm$				
$l = 0\ nm$	0.1700	0.2253	0.1342	0.1956
$l = 1\ nm$	0.1709 (+0.502%)	0.2265 (+0.517%)	0.1348 (+0.462%)	0.1966 (+0.506%)
$l = 2\ nm$	0.1734 (+1.992%)	0.2299 (+2.051%)	0.1366 (+1.836%)	0.1995 (+2.010%)
$l = 3\ nm$	0.1776 (+4.429%)	0.2356 (+4.559%)	0.1396 (+4.085%)	0.2043 (+4.468%)
$l = 4\ nm$	0.1832 (+7.749%)	0.2432 (+7.972%)	0.1438 (+7.154%)	0.2109 (+7.815%)
$W_{max} = 0.02$, $\mu = 0\ nm$				
□ = □ □□	0.1900	0.2433	0.1625	0.2164
□ = □ □□	0.1908 (+0.403%)	0.2444 (+0.444%)	0.1630 (+0.317%)	0.2173 (+0.414%)
□ = □ □□	0.1930 (+1.601%)	0.2476 (+1.763%)	0.1645 (+1.256%)	0.2200 (+1.647%)
□ = □ □□	0.1968 (+3.566%)	0.2528 (+3.926%)	0.1670 (+2.805%)	0.2244 (+3.668%)
□ = □ □□	0.2019 (+6.258%)	0.2600 (+6.879%)	0.1705 (+4.935%)	0.2303 (+6.434%)

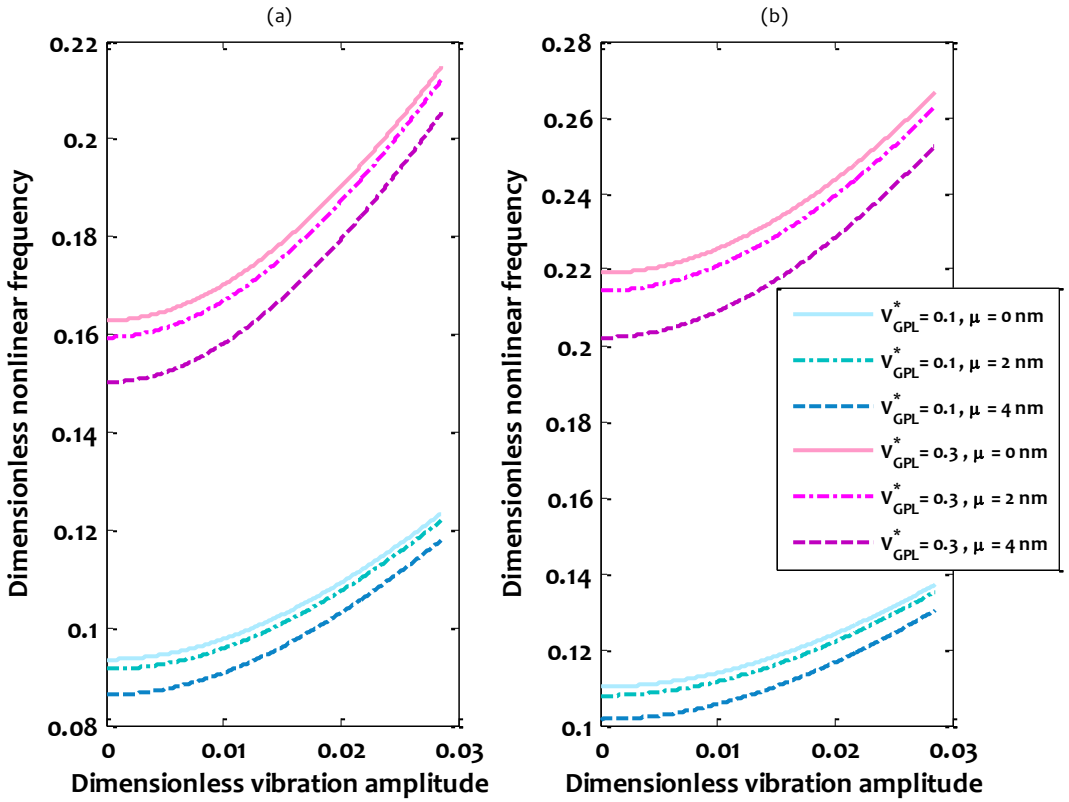

Figure 5. *Variation of nonlinear frequency with vibration amplitude of multilayer GPLRC nanobeams corresponding to various small scale parameters and GPL dispersion patterns ($l = 0$ nm): (a) U-GPLRC nanobeam, (b) X-GPLRC nanobeam*

In Figures 5 and 6, the influence of GPL weight fraction on the nonlinear vibrational response of multilayer U-GPLRC nanobeams including nonlocality and strain gradient size dependency, respectively, is shown. It can be seen that by increasing the value of GPL weight fraction, both types of the small scale effect become more significant. As a result, the gap between the curves corresponding to various small scale parameters increases. Also, for multilayer U-GPLRC nanobeams with higher GPL weight fraction, the slope of frequency-amplitude variation increases. In other words, the influence of GPL weight fraction on the nonlinear frequency of multilayer functionally graded nanobeams is more significant at lower vibration amplitude.

Tabulated in Table 4 are the dimensionless nonlinear frequencies of multilayer functionally graded GPLRC nanobeams with different GPL weight fractions and corresponding to various values of vibration amplitude and small scale parameters. It is found that for U-GPLRC nanobeam, the value of GPL weight fraction has no influence on the significance of the size effects on the nonlinear frequency at specific vibration amplitude. However, by increasing the value of GPL weight fraction, both of the nonlocal and strain gradient size dependencies in the large amplitude nonlinear frequency of X-GPLRC and A-GPLRC nanobeams enhances, but for O-GPLRC nanobeam, this pattern is vice versa.

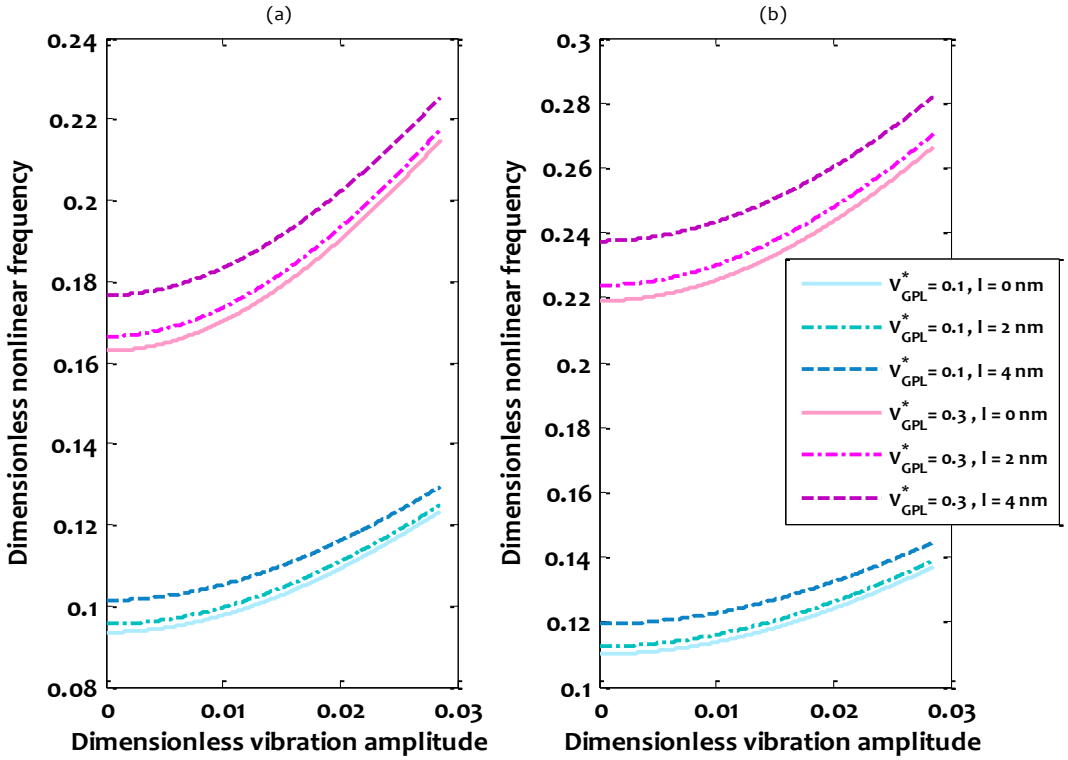

Figure 6. *Variation of nonlinear frequency with vibration amplitude of multilayer GPLRC nanobeams corresponding to various small scale parameters and GPL dispersion patterns ($\mu = 0\ nm$): (a) U-GPLRC nanobeam, (b) X-GPLRC nanobeam.*

Figure 7 represents the frequency-amplitude variation of multilayer functionally graded GPLRC nanobeams containing GPL nanofillers with different length to thickness ratio. It is demonstrated by increasing the length to thickness ratio of GPL nanofillers, the both of nonlocality and strain gradient size dependencies play more important role in the nonlinear vibration response. Moreover, it is observed that by increasing the value of L_{GPL}/h_{GPL}, the nonlinear frequency as well as the slope of frequency-amplitude variation of the multilayer GPLRC nanobeams increases.

5. CONCLUDING REMARKS

Size-dependent large amplitude nonlinear vibration of multilayer functionally graded GPLRC nanobeams was studied in a more comprehensive way. To this purpose, the nonlocal strain gradient elasticity theory including both of the hardening-stiffness and softening-stiffness size effects was implemented into the third-order shear deformation beam theory. Using an improved perturbation technique in conjunction with the Galerkin method, an explicit analytical expression for nonlocal strain gradient nonlinear frequency of multilayer functionally graded GPLRC nanobeams.

It was seen that the nonlocality causes the slope increase of the variation of nonlinear frequency to linear frequency ratio with vibration amplitude, while the strain gradient size dependency leads to reduce it. Also, by moving to deeper nonlinear regime (increasing the vibration amplitude of nanobeam), both types of the small scale effect plays more important role in the value of nonlinear frequency to linear frequency ratio of multilayer functionally graded GPLRC nanobeams. It was presented that for all GPL dispersion patterns and various vibration amplitudes,

the strain gradient size effect on the nonlinear frequency of GPLRC nanobeams is a bit more than that of nonlocality with the same value of small scale parameter.

Table 4. *Size-dependent dimensionless nonlinear frequencies of multilayer GPLRC nanobeams with different GPL weight fraction and corresponding to various small scale parameters and vibrations amplitudes.*

V^*_{GPL}	Small scale parameters (nm)	U-GPLRC	X-GPLRC	O-GPLRC	A-GPLRC
			$W_{max}=0$		
0.1	$l=0\ ,\ \mu=0$	0.0935	0.1101	0.0764	0.0957
	$l=0\ ,\ \mu=2$	0.0915 (-2.125%)	0.1078 (-2.125%)	0.0748 (-2.125%)	0.0936 (-2.125%)
	$l=0\ ,\ \mu=4$	0.0862 (-7.765%)	0.1016 (-7.765%)	0.0704 (-7.765%)	0.0882 (-7.765%)
	$l=2\ ,\ \mu=0$	0.0955 (+2.170%)	0.1125 (+2.170%)	0.0780 (+2.170%)	0.0977 (+2.170%)
	$l=4\ ,\ \mu=0$	0.1013 (+8.419%)	0.1194 (+8.419%)	0.0828 (+8.419%)	0.1037 (+8.419%)
0.3	$l=0\ ,\ \mu=0$	0.1628	0.2190	0.1233	0.1882
	$l=0\ ,\ \mu=2$	0.1594 (-2.125%)	0.2143 (-2.125%)	0.1207 (-2.125%)	0.1842 (-2.125%)
	$l=0\ ,\ \mu=4$	0.1502 (-7.765%)	0.2020 (-7.765%)	0.1137 (-7.765%)	0.1735 (-7.765%)
	$l=2\ ,\ \mu=0$	0.1664 (+2.170%)	0.2237 (+2.170%)	0.1259(+2.170%)	0.1922 (+2.170%)
	$l=4\ ,\ \mu=0$	0.1765 (+8.419%)	0.2374 (+8.419%)	0.1337 (+8.419%)	0.2040 (+8.419%)
			$W_{max}=0.01$		
0.1	$l=0\ ,\ \mu=0$	0.0976	0.1137	0.0815	0.0998
	$l=0\ ,\ \mu=2$	0.0957 (-1.947%)	0.1115 (-1.990%)	0.0800 (-1.864%)	0.0979 (-1.950%)
	$l=0\ ,\ \mu=4$	0.0907 (-7.099%)	0.1055 (-7.262%)	0.0760 (-6.788%)	0.0927 (-7.111%)
	$l=2\ ,\ \mu=0$	0.0995 (+1.992%)	0.1161 (+2.036%)	0.0831 (+1.909%)	0.1018 (+1.995%)
	$l=4\ ,\ \mu=0$	0.1052 (+7.749%)	0.1227 (+7.913%)	0.0876 (+7.432%)	0.1076 (+7.760%)
0.3	$l=0\ ,\ \mu=0$	0.1700	0.2253	0.1342	0.1956
	$l=0\ ,\ \mu=2$	0.1667 (-1.947%)	0.2208 (-2.006%)	0.1318 (-1.791%)	0.1918 (-1.964%)
	$l=0\ ,\ \mu=4$	0.1580 (-7.099%)	0.2088 (-7.320%)	0.1254 (-6.516%)	0.1816 (-7.165%)
	$l=2\ ,\ \mu=0$	0.1734 (+1.992%)	0.2299 (+2.051%)	0.1366 (+1.836%)	0.1995 (+2.010%)
	$l=4\ ,\ \mu=0$	0.1832 (+7.749%)	0.2432 (+7.972%)	0.1438 (+7.154%)	0.2109 (+7.815%)
			$W_{max}=0.02$		
0.1	$l=0\ ,\ \mu=0$	0.1091	0.1240	0.0952	0.1113
	$l=0\ ,\ \mu=2$	0.1074 (-1.558%)	0.1219 (-1.674%)	0.0939 (-1.363%)	0.1096 (-1.565%)
	$l=0\ ,\ \mu=4$	0.1029 (-5.650%)	0.1164 (-6.083%)	0.0905 (-4.930%)	0.1050 (-5.678%)
	$l=2\ ,\ \mu=0$	0.1108 (+1.601%)	0.1261 (+1.718%)	0.0966 (+1.403%)	0.1131 (+1.608%)
	$l=4\ ,\ \mu=0$	0.1159 (+6.258%)	0.1323 (+6.707%)	0.1005 (+5.501%)	0.1183 (+6.287%)
0.3	$l=0\ ,\ \mu=0$	0.1900	0.2433	0.1625	0.2164
	$l=0\ ,\ \mu=2$	0.1870 (-1.558%)	0.2391 (-1.720%)	0.1605 (-1.219%)	0.2130 (-1.603%)
	$l=0\ ,\ \mu=4$	0.1793 (-5.650%)	0.2281 (-6.249%)	0.1553 (-4.399%)	0.2038 (-5.819%)
	$l=2\ ,\ \mu=0$	0.1930 (+1.601%)	0.2476 (+1.763%)	0.1645 (+1.256%)	0.2200 (+1.647%)
	$l=4\ ,\ \mu=0$	0.2019 (+6.258%)	0.2600 (+6.879%)	0.1705 (+4.935%)	0.2303 (+6.434%)

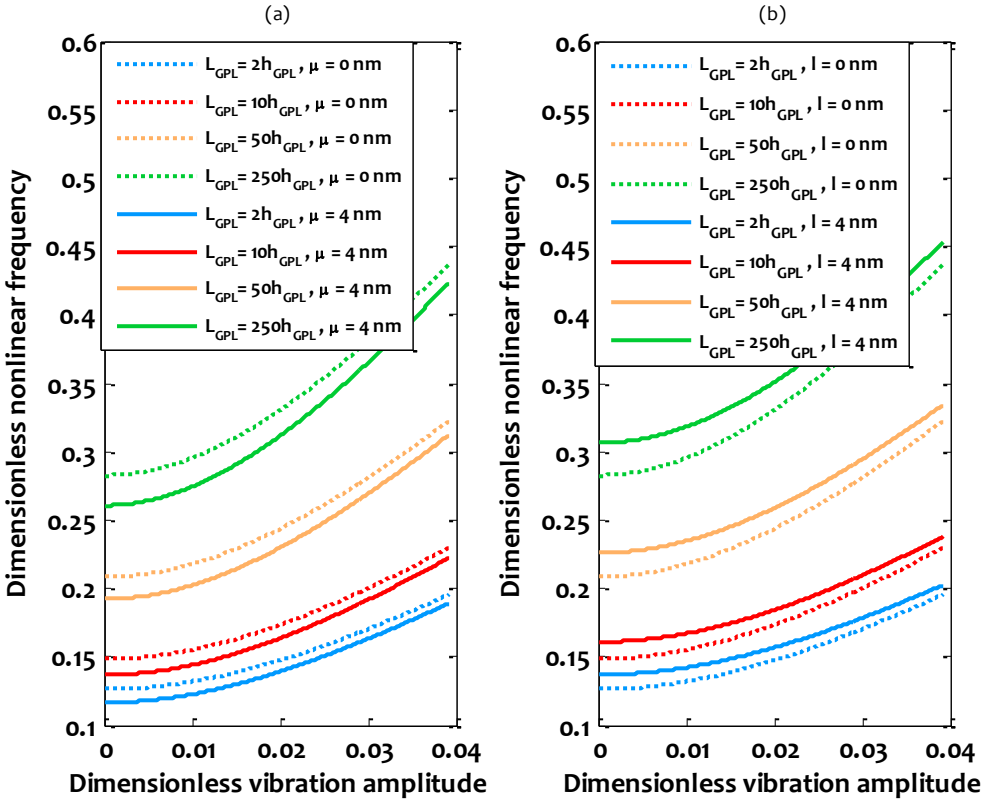

Figure 7. *Variation of nonlinear frequency with vibration amplitude of multilayer U-GPLRC nanobeams including GPL nanofillers with different length to thickness ratios ($V^*_{GPL} = 0.3$): (a) $l = 0\ nm$, (b) $\mu = 0\ nm$.*

Moreover, it was observed that at zero vibration amplitude, the pattern of GPL dispersion has no influence on the significance of the size dependencies, so the percentages are similar corresponding to each value of small scale parameter. However, by taking the large vibration amplitude into account, both of the nonlocality and strain gradient size effects on the nonlinear frequency of O-GPLRC and X-GPLRC nanobeams are minimum and maximum, respectively.

It was revealed that for U-GPLRC nanobeam, the value of GPL weight fraction has no influence on the significance of the size effects on the nonlinear frequency at specific vibration amplitude. However, by increasing the value of GPL weight fraction, both of the nonlocal and strain gradient size dependencies in the large amplitude nonlinear frequency of X-GPLRC and A-GPLRC nanobeams enhances, but for O-GPLRC nanobeam, this pattern is vice versa. Additionally, it was shown that by increasing the length to thickness ratio of GPL nanofillers, the both of nonlocality and strain gradient size dependencies play more important role in the nonlinear vibration response.

ACKNOWLEDGEMENT

The work presented in this paper was supported by a grant from the Iran National Science Foundation (INSF) with contract number of 95848881.

REFERENCES

1. Soleimani M., Ghorbani M., Salahi S., (2016). "Antibacterial activity of polypyrrole-chitosan nanocomposite: Mechanism of action", *International Journal of Nanoscience and Nanotechnology*, 12: 191-197.

2. Habibi B., Ayazi Z., Zalvand F., (2017). "Electrochemical behavior and determination of phenylephrine at the multi-walled carbon nanotubes/ionic liquid nanocomposite modified electrode in the presence of acetaminophen", *International Journal of Nanoscience and Nanotechnology*, 13: 203-218.
3. Ahmadi-Moghadam B., Taheri F., (2015). "Influence of graphene nanoplatelets on modes I, II and III interlaminar fracture toughness of fiber-reinforced polymer composites", *Engineering Fracture Mechanics*, 143: 97-107.
4. Tang Y., Jia Y., Alva G., Huang X., Fang G., (2016). "Synthesis, characterization and properties of palmitic acid/high density polyethylene/graphene nanoplatelets composites as form-stable phase change materials", *Solar Energy Materials and Solar Cells*, 155: 421-429.
5. Scaffaro R., Botta L., Maio A., Gallo G., (2017). "PLA graphene nanoplatelets nanocomposites: Physical properties and release kinetics of an antimicrobial agent", *Composites Part B: Engineering*, 109: 138-146.
6. Yang J., Tang L. -S., Bao R. -Y., Bai L., Liu Z. -Y., Yang W., Xie B. -H., Yang M. -B., (2017). "Largely enhanced thermal conductivity of poly (ethylene glycol)/boron nitride composite phase change materials for solar-thermal-electric energy conversion and storage with very low content of graphene nanoplatelets", *Chemical Engineering Journal*, 315: 481-490.
7. Feng C., Kitipornchai S., Yang J., (2017). "Nonlinear free vibration of functionally graded polymer composite beams reinforced with graphene nanoplatelets", *Engineering Structures*, 140: 110-119.
8. Zhao Z., Feng C., Wang Y., Yang J., (2017). "Bending and vibration analysis of functionally graded trapezoidal nanocomposite plates reinforced with graphene nanoplatelets (GPLs)", *Composite Structures*, 180: 799-808.
9. Wang Y., Feng C., Zhao Z., Yang J., (2018). "Buckling of graphene platelet reinforced composite cylindrical shell with cutout, *International Journal of Structural Stability and Dynamics*, 18: 1850040.
10. Feng C., Wang Y., Yang J., (2018). "Effects of reorientation of graphene platelets (GPLs) on Young's modulus of polymer composites under bi-axial stretching", *Nanomaterials* 8: 27.
11. Sun R., Li L., Feng C., Kitipornchai S., Yang J., (2018). "Tensile behavior of polymer nanocomposite reinforced with graphene containing defects", *European Polymer Journal* 98: 475-482.
12. Song M., Kitipornchai S., Yang J., (2017). "Free and forced vibrations of functionally graded polymer composite plates reinforced with graphene nanoplatelets", *Composite Structures*, 159: 579-588.
13. Feng C., Kitipornchai S., Yang J., (2017). "Nonlinear bending of polymer nanocomposite beams reinforced with non-uniformly distributed graphene platelets (GPLs) ", *Composites Part B: Engineering*, 110: 132-140.
14. Yang J., Wu H., Kitipornchai S., (2017). "Buckling and postbuckling of functionally graded multilayer graphene platelet-reinforced composite beams", *Composite Structures*, 161: 111-118.
15. Fu Y., Du H., Zhang S., (2003). "Functionally graded TiN/TiNi shape memory alloy films", *Materials Letters*, 57: 2995-2999.
16. Fu Y., Du H., Huang W., Zhang S., Hu M., (2004). "TiNi-based thin films in MEMS applications: a review", *Sensors and Actuators A: Physical*, 112: 395-408.
17. Zhang B., He Y., Liu D., Gan Z., Shen L., (2013). "A non-classical Mindlin plate finite element based on a modified couple stress theory", *European Journal of Mechanics – A/Solids*, 42: 63-80.
18. Akgoz B., Civalek O., (2013). "Free vibration analysis of axially functionally graded tapered Bernoulli–Euler microbeams based on the modified couple stress theory", *Composite Structures*, 98: 314-322.
19. Ramezani S., (2013). "Nonlinear vibration analysis of micro-plates based on strain gradient elasticity theory", *Nonlinear Dynamics*, 73: 1399-1421.
20. Reddy J. N., El-Borgi S., Romanoff J., (2014). "Non-linear analysis of functionally graded microbeams using Eringen′s non-local differential model", *International Journal of Non-Linear Mechanics*, 67: 308-318.
21. Sahmani S., Aghdam M. M., Bahrami M., (2015). "On the postbuckling behavior of geometrically imperfect cylindrical nanoshells subjected to radial compression including surface stress effects", *Composite Structures*, 131: 414-424.
22. Shojaeian M., Tadi Beni Y., (2015). "Size-dependent electromechanical buckling of functionally graded electrostatic nano-bridges", *Sensors and Actuators A: Physical*, 232: 49-62.
23. Li Y. S., Pan E., (2015). "Static bending and free vibration of a functionally graded piezoelectric microplate based on the modified couple-stress theory", *International Journal of Engineering Science*, 97: 40-59.
24. Jung W. -Y., Han S. -C., (2015). "Static and eigenvalue problems of Sigmoid functionally graded materials (S-FGM) micro-scale plates using the modified couple stress theory", *Applied Mathematical Modelling*, 39: 3506-3524.
25. Sahmani S., Aghdam M. M., Bahrami M., (2015). "On the free vibration characteristics of postbuckled third-order shear deformable FGM nanobeams including surface effects", *Composite Structures*, 121: 377-385.
26. Kiani K., (2016). "Free dynamic analysis of functionally graded tapered nanorods via a newly developed nonlocal surface energy-based integro-differential model", *Composite Structures*, 139: 151-166.

27. Sahmani S., Aghdam M. M., Akbarzadeh A. H., (2016). "Size-dependent buckling and postbuckling behavior of piezoelectric cylindrical nanoshells subjected to compression and electrical load", *Materials & Design*, 105: 341-351.
28. Mashrouteh S., Sadri M., Younesian D., Esmailzadeh E., (2016). "Nonlinear vibration analysis of fluid-conveying microtubes", Nonlinear Dynamics, 85: 1007-1021.
29. Sahmani S., Aghdam M. M., (2017). "Nonlocal strain gradient beam model for nonlinear vibration of prebuckled and postbuckled multilayer functionally graded GPLRC nanobeams", *Composite Structures*, 179: 77-88.
30. Nguyen H. X., Nguyen T. N., Abdel-Wahab M., Bordas S. P. A., Nguyen-Xuan H., Vo T.P., (2017). "A refined quasi-3D isogeometric analysis for functionally graded microplates based on the modified couple stress theory", *Computer Methods in Applied Mechanics and Engineering*, 313: 904-940.
31. Sahmani S., Aghdam M. M., (2017). "A nonlocal strain gradient hyperbolic shear deformable shell model for radial postbuckling analysis of functionally graded multilayer GPLRC nanoshells", *Composite Structures*, 178: 97-109.
32. Sahmani S., Aghdam M. M., (2017). "Nonlinear instability of axially loaded functionally graded multilayer graphene platelet-reinforced nanoshells based on nonlocal strain gradient elasticity theory", *International Journal of Mechanical Science*, 131: 95-106.
33. Sahmani S., Aghdam M. M., (2017). "Axial postbuckling analysis of multilayer functionally graded composite nanoplates reinforced with GPLs based on nonlocal strain gradient theory", *The European Physical Journal Plus*, 132: 490.
34. Simsek M., Aydin M., (2017). "Size-dependent forced vibration of an imperfect functionally graded (FG) microplate with porosities subjected to a moving load using the modified couple stress theory", *Composite Structures*, 160: 408-421.
35. Sahmani S., Aghdam M. M., Bahrami M., (2017). "An efficient size-dependent shear deformable shell model and molecular dynamics simulation for axial instability analysis of silicon nanoshells", *Journal of Molecular Graphics and Modelling*, 77: 263-279.
36. Sahmani S., Fattahi A. M., (2017). "An anisotropic calibrated nonlocal plate model for biaxial instability analysis of 3D metallic carbon nanosheets using molecular dynamics simulations", *Materials Research Express*, 4: 065001.
37. Sahmani S., Fattahi A. M., (2017). "Nonlocal size dependency in nonlinear instability of axially loaded exponential shear deformable FG-CNT reinforced nanoshells under heat conduction", *The European Physical Journal Plus*, 132: 231.
38. Sahmani S., Fattahi A. M., (2017). "Size-dependent nonlinear instability of shear deformable cylindrical nanopanels subjected to axial compression in thermal environments", *Microsystem Technologies*, 23: 4717-4731.
39. Sahmani S., Fattahi A. M., (2017). "Thermo-electro-mechanical size-dependent postbuckling response of axially loaded piezoelectric shear deformable nanoshells via nonlocal elasticity theory", *Microsystem Technologies*, 23: 5105-5119.
40. Fattahi A. M., Sahmani S., (2017). "Nonlocal temperature-dependent postbuckling behavior of FG-CNT reinforced nanoshells under hydrostatic pressure combined with heat conduction", *Microsystem Technologies*, 23: 5121-5137.
41. Fattahi A. M., Sahmani S., (2017). "Size dependency in the axial postbuckling behavior of nanopanels made of functionally graded material considering surface elasticity", *Arabian Journal for Science and Engineering*, 42: 4617-4633.
42. Sahmani S., Fattahi A. M., (2017). "Imperfection sensitivity of the size-dependent nonlinear instability of axially loaded FGM nanopanels in thermal environments", *Acta Mechanica*, 228: 3789-3810.
43. Lim C.W., Zhang G., Reddy J.N., (2015). "A higher-order nonlocal elasticity and strain gradient theory and its applications in wave propagation", *Journal of Mechanics and Physics of Solids*, 78: 298-313.
44. Li L., Hu Y., (2015). "Buckling analysis of size-dependent nonlinear beams based on a nonlocal strain gradient theory", International Journal of Engineering Science, 97: 84-94.
45. Li L., Hu Y., (2016). "Wave propagation in fluid-conveying viscoelastic carbon nanotubes based on nonlocal strain gradient theory", *Computational Materials Science*, 112: 282-288.
46. Yang W. D., Yang F. P., Wang X., (2016). "Coupling influences of nonlocal stress and strain gradients on dynamic pull-in of functionally graded nanotubes reinforced nano-actuator with damping effects", *Sensors and Actuators A: Physical*, 248: 10-21.
47. Li, L., Li, X., Hu Y., (2016). "Free vibration analysis of nonlocal strain gradient beams made of functionally graded material", *International Journal of Engineering Science*, 102: 77-92.
48. Simsek M., (2016). "Nonlinear free vibration of a functionally graded nanobeam using nonlocal strain gradient theory and a novel Hamiltonian approach", *International Journal of Engineering Science*, 105: 10-21.

49. Farajpour A., Haeri Yazdi M. R., Rastgoo A., Mohammadi M., (2016). "A higher-order nonlocal strain gradient plate model for buckling of orthotropic nanoplates in thermal environment", *Acta Mechanica*, 227: 1849-1867.
50. Sahmani S., Aghdam M. M., (2017). "Size-dependent axial instability of microtubules surrounded by cytoplasm of a living cell based on nonlocal strain gradient elasticity theory", *Journal of Theoretical Biology*, 422: 59-71.
51. Sahmani S., Aghdam M. M., (2017). "Nonlinear vibrations of pre-and post-buckled lipid supramolecular micro/nano-tubules via nonlocal strain gradient elasticity theory", *Journal of Biomechanics*, 65: 49-60.
52. Sahmani S., Aghdam M. M., (2018). "Nonlocal strain gradient beam model for postbuckling and associated vibrational response of lipid supramolecular protein micro/nano-tubules", *Mathematical Biosciences*, 295: 24-35.
53. Lu L., Guo X., Zhao J., (2017). "A unified nonlocal strain gradient model for nanobeams and the importance of higher order terms", *International Journal of Engineering Science*, 119: 265-277.
54. Sahmani S., Aghdam M. M., (2018). "Nonlocal strain gradient shell model for axial buckling and postbuckling analysis of magneto-electro-elastic composite nanoshells", *Composites Part B: Engineering*, 132: 258-274.
55. Sahmani S., Aghdam M. M., Rabczuk T., (2018). "A unified nonlocal strain gradient plate model for nonlinear axial instability of functionally graded porous micro/nano-plates reinforced with graphene platelets", *Materials Research Express*, 5: 045048.
56. Sahmani S., Aghdam M. M., Rabczuk T., (2018). "Nonlocal strain gradient plate model for nonlinear large-amplitude vibrations of functionally graded porous micro/nano-plates reinforced with GPLs", *Composite Structures*, 198: 51-62.
57. Sahmani S., Fattahi A. M., (2018). "Small scale effects on buckling and postbuckling behaviors of axially loaded FGM nanoshells based on nonlocal strain gradient elasticity theory", *Applied Mathematics and Mechanics*, 39: 561-580.
58. Zhu X., Li L., (2017). "Closed form solution for a nonlocal strain gradient rod in tension", *International Journal of Engineering Science*, 119: 16-28.
59. Zhu X., Li L., (2017). "On longitudinal dynamics of nanorods", *International Journal of Engineering Science*, 120: 129-145.
60. Halpin J. C., Kardos J. L., (1976). "The Halpin-Tsai equations: a review", *Polymer Engineering & Science*, 16: 344-352.
61. Hejazi S. M., Abtahi S. M., Safaie F., (2016). "Investigation of thermal stress distribution in fiber reinforced roller compacted concrete pavements", *Journal of Industrial Textile*, 45: 869-914.
62. Shen H. -S., Chen X., Guo L., Wu L., Huang X. -L., (2015). "Nonlinear vibration of FGM doubly curved panels resting on elastic foundations in thermal environments", *Aerospace Science and Technology*, 47: 434-446.
63. Shen H. -S. Yang D. -Q., (2015). "Nonlinear vibration of functionally graded fiber reinforced composite laminated beams with piezoelectric fiber reinforced composite actuators in thermal environments", *Engineering Structures*, 90: 183-192.
64. Shen H. -S., Wang H., (2015). "Nonlinear bending of FGM cylindrical panels resting on elastic foundations in thermal environments", *European Journal of Mechanics – A/Solids*, 49: 49-59.
65. Shen H. -S., Chen X., Huang X. -L., (2016). "Nonlinear bending and thermal postbuckling of functionally graded fiber reinforced composite laminated beams with piezoelectric fiber reinforced composite actuators", *Composites Part B: Engineering*, 90: 326-335.
66. Sahmani S., Aghdam M. M., (2017). "Size-dependent nonlinear bending of micro/nano-beams made of nanoporous biomaterials including a refined truncated cube cell", *Physics Letters A*, 381: 3818-3830.
67. Sahmani S. Aghdam M. M., (2017). "Imperfection sensitivity of the size-dependent postbuckling response of pressurized FGM nanoshells in thermal environments", *Archives of Civil and Mechanical Engineering*, 17: 623-638.
68. Sahmani S., Aghdam M. M., Rabczuk T., (2018). "Nonlinear bending of functionally graded porous micro/nano-beams reinforced with graphene platelets based upon nonlocal strain gradient theory", *Composite Structures*, 186: 68-78.
69. Sahmani S., Aghdam M. M., (2018). "Nonlinear instability of hydrostatic pressurized microtubules surrounded by cytoplasm of a living cell including nonlocality and strain gradient microsize dependency", *Acta Mechanica*, 229: 403-420.
70. Sahmani S., Aghdam M. M., (2018). "Thermo-electro-radial coupling nonlinear instability of piezoelectric shear deformable nanoshells via nonlocal elasticity theory", *Microsystem Technologies*, 24: 1333-1346.
71. Sahmani S., Khandan A., Saber-Samandari S., Aghdam M. M., (2018). "Vibrations of beam-type implants made of 3D printed bredigite-magnetite bio-nanocomposite scaffolds under axial compression: Application, communication and simulation", *Ceramics International*, 44: 11282-11291.

72. Sahmani S., Khandan A., Saber-Samandari S., Aghdam M. M., (2018). "Nonlinear bending and instability analysis of bioceramics composed with magnetite nanoparticles: Fabrication, characterization, and simulation", *Ceramics International*, Article in Press.
73. Liu F., Ming P., Li J., (2007). "Ab initio calculation of ideal strength and phonon instability of graphene under tension", *Physical Review B*, 76: 064120.
74. Rafiee M. A., Rafiee J., Wang Z., Song H., Yu Z. -Z., Koratkar N., (2009). "Enhanced mechanical properties of nanocomposites at low graphene content", *ASC Nano*, 3: 3884-3890.
75. Yang J., Ke L. L., Kitipornchai S., (2010). "Nonlinear free vibration of single-walled carbon nanotubes using nonlocal Timoshenko beam theory", *Physica E*, 42: 1727-1735.